DOI: 10.1002/ejic.201100793

γ-AlOOH Nanomaterials with Regular Shapes: Hydrothermal Fabrication and $Cr_2O_7^{2-}$ Adsorption

Li Zhang,[a] Xiuling Jiao,*[a] Dairong Chen,*[a] and Mingxia Jiao[a]

Keywords: γ-AlOOH / Nanostructures / Hydrothermal synthesis / Adsorption

Well-defined boehmite (γ-AlOOH) nanomaterials with regular shapes, which include nanorods, nanobelts, and nanoplates, were prepared by hydrothermal reactions of γ-AlOOH nanoparticles, to which H_2SO_4, CH_3COOH, and HCl were added to regulate the shape of the products. The formation of the nanomaterials with different shapes could be attributed to adsorption of SO_4^{2-}, CH_3COO^-, and Cl^- on the crystal planes, which affected the oriented aggregation of the raw γ-AlOOH nanoparticles and the growth of the aggregates. The difference in the adsorption abilities of the acidic anions resulted in the different shapes of the products. The corresponding shape-retained γ-Al_2O_3 nanomaterials were obtained after calcination. Furthermore, the differently shaped nanomaterials exhibited different adsorption capabilities for $Cr_2O_7^{2-}$ in aqueous solution, and the nanobelts showed an adsorption of up to 95.5 %. The exposed crystal facet of the γ-AlOOH nanomaterials is an important factor that affects the adsorption ability.

Introduction

Boehmite (γ-AlOOH) attracts widespread attention, because it is widely used as catalyst,[1] adsorbent,[2] and composite.[3] γ-AlOOH can also be used as a crucial precursor for the synthesis of nanoscale γ-Al_2O_3, as the shape can be retained during the phase transformation from γ-AlOOH to γ-Al_2O_3.[4] In previous reports, the design and synthesis of γ-AlOOH nanomaterials have attracted great interest because of their size- and shape-dependent properties. For example, the photoluminescence spectra of γ-AlOOH nanoplatelets and nanowires display different emission bands according to their distinct sizes and morphologies.[5] The core/shell microspheres exhibited superior adsorption abilities compared with commercial γ-AlOOH nanoparticles.[6] To date, many γ-AlOOH nanomaterials with different shapes such as fibers,[7] rods,[4,8] tubes,[7b,9] and plates[8a,10] have been prepared. Hydrothermal or solvothermal routes,[7,8,11,12] sol–gel techniques,[13] and the thermal decomposition of organic complexes[14] are usually applied to synthesize γ-AlOOH nanomaterials. The hydro/solvothermal route uses moderate conditions and allows easy control of the shape and crystallinity of the products. Surfactants, organic additives or the hydrothermal conditions can be adjusted to control the particle morphology;[7,8,11,12,15] however, the detailed shape-control mechanism and the size- and shape-dependent properties need to be further investigated.

Initial nanoparticle materials with specific morphologies and new properties are of great interest in the area of materials synthesis and device fabrication.[16] The assembly of the initial nanoparticles generally results in significant changes to the morphology, dimensions, crystallographic structure, and properties.[17] Many nanomaterials with various shapes have been fabricated by oriented attachment of nanoparticles;[18–23] however, the assembly of γ-AlOOH nanoparticles has rarely been reported. Herein, we report the synthesis of γ-AlOOH nanomaterials with regular shapes, which include nanorods, nanobelts, and nanoplates, through the assembly of γ-AlOOH nanoparticles that uses H_2SO_4, CH_3COOH, and HCl as shape-directing agents, and the detailed fabrication mechanism is investigated. Furthermore, the product can easily be scaled up to a few kilograms, which provides a simple and cheap method for the controllable large-scale preparation of γ-AlOOH nanomaterials with regular shapes. In addition, the adsorption properties of the products were investigated. The materials exhibit shape-dependent adsorption capabilities for $Cr_2O_7^{2-}$ in aqueous solution.

$Cr_2O_7^{2-}$ is the most toxic primary pollutant in water that threatens the survival of mankind.[12c] In previous reports, boehmite materials have proven to be useful in the treatment of $Cr_2O_7^{2-}$-containing waste water.[2] It has been reported that the efficient removal of $Cr_2O_7^{2-}$ from aqueous solutions by γ-AlOOH was due to the relatively large surface and mesoporous structure of the material; however, the effect of the exposed crystal facet was not considered.[2,6,12c] In this study, γ-AlOOH nanomaterials with different shapes

---

[a] Key Laboratory for Special Functional Aggregate Materials, Education Ministry, School of Chemistry and Chemical Engineering, Shandong University
Jinan 250100, P. R. China
Fax: +86-531-88364281
E-mail: cdr@sdu.edu.cn

Supporting information for this article is available on the WWW under http://dx.doi.org/10.1002/ejic.201100793.

from similar hydrothermal systems and the same γ-AlOOH nanoparticle precursor provide the opportunity to investigate the effect of the exposed facet on the adsorption properties, and it is revealed that the (1 0 0) facet exhibits superior adsorption properties for $Cr_2O_7^{2-}$ in aqueous solution, in which the nanobelts showed an adsorption of 95.5%.

Results and Discussion

Morphology and Structure

Figure 1 shows the XRD patterns and scanning electron microscopy (SEM) images of the products formed in the presence of H_2SO_4, CH_3COOH, and HCl. The reflections of all the products were readily indexed to the orthorhombic boehmite phase γ-AlOOH (JCPDS No. 83-2384), and no characteristic peaks of impurities are observed. In the presence of H_2SO_4, the XRD peaks of the product are much weaker than those of others, which indicates that the acid affects the crystallinity of the product, and the lower intensity and broadening of the peaks is attributed to smaller crystal size. SEM images indicate that nanorods with a diameter of 8–35 nm and length of 100–400 nm were produced in the H_2SO_4 system. Nanobelts with a thickness of 15–25 nm, width of 30–70 nm, and length of 100–800 nm with the arrow-headed ends were formed in the CH_3COOH system. Square nanoplates with a thickness of 20–40 nm and side length of 55–155 nm were obtained from the HCl system.

Figure 2 gives the TEM images of the products, which are in accord with the SEM images. The high-resolution (HR)TEM images of a nanorod, nanobelt, and nanoplate show the continuous lattice fringes, which demonstrates their single-crystalline nature. For the nanorods, the interplanar distance is ca. 0.199 nm, which could be ascribed to the (0 6 0) plane of γ-AlOOH, and the corresponding fast Fourier transform (FFT) pattern (Figure 2d, inset) shows the growth direction along [0 0 1]. For the nanobelts, interplanar distances of 0.286 and 0.234 nm could be assigned to the (0 0 1) and (0 3 1) planes of γ-AlOOH, respectively, which was confirmed by the FFT pattern (Figure 2e, inset). The long axis of the nanobelt is parallel to the [0 0 1] direction, and the wide plane of the nanobelt is perpendicular to the [1 0 0] direction. For the nanoplates, interplanar distances of 0.244 and 0.234 nm were assigned to the (0 5 0) and (0 3 1) planes of γ-AlOOH, and the FFT pattern (Figure 2f, inset) reveals that the preferred surface of the nanoplate is the (1 0 0) plane. Although the HRTEM images reveal that the products are single crystals, the obvious difference in contrast and the defects observed imply the oriented-attachment growth of the γ-AlOOH nanoparticles.

FTIR spectra of the raw material and the products show absorptions at almost the same wavenumbers but with different intensities. The broad absorptions at 3095 and 3305 cm^{-1} are attributed to the symmetric and asymmetric stretching vibrations of –OH groups (Figure 3),[24] and those at 2100 and 1970 cm^{-1} are attributed to the vibrational overtones of the surface –OH groups of γ-AlOOH.[25] The five absorption bands at around 1165, 1075, 745, 625, and 487 cm^{-1} are assigned to the O–H bending, (HO)–Al=O asymmetric stretching, (AlO)–O–H angle bending, (OH)–Al=O angle bending, and O=Al–(OH) angle deformation (wagging) vibrations, respectively, which are the fundamental modes of the vibrations of nonlinear boehmite.[2,26] These results indicate that only some absorbed water molecules and hydroxy groups are on the surface of the products.

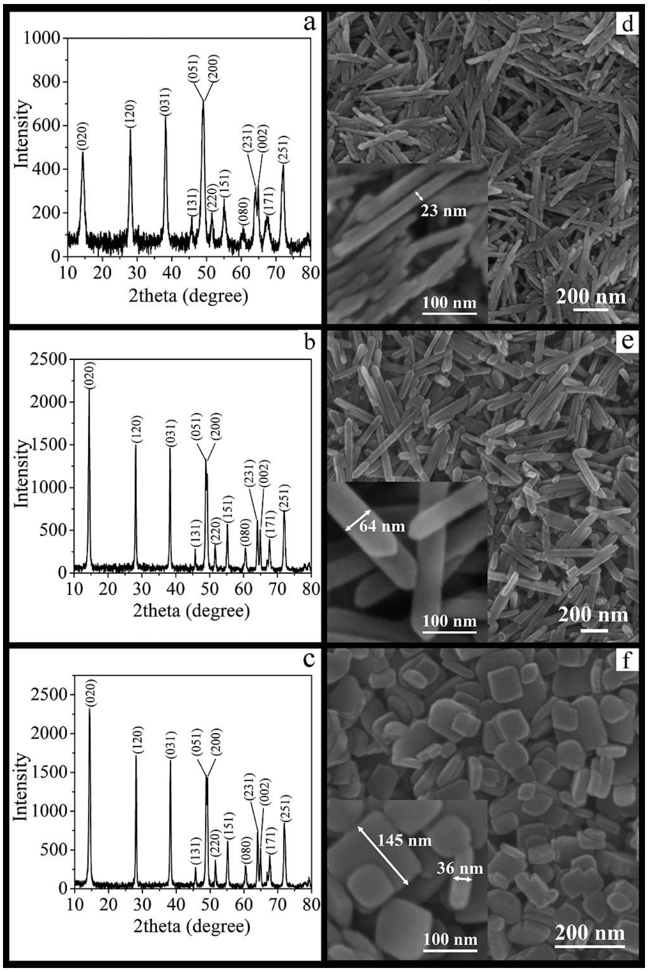

Figure 1. XRD patterns and SEM images of the products formed in the presence of H_2SO_4 (a, d), CH_3COOH (b, e), and HCl (c, f).

There are three mass-loss steps in the thermogravimetric analysis (TGA) curves of the nanorods, nanobelts, and nanoplates: below 200 °C, from 200–800 °C, and above 800 °C (Figure 4). The mass losses below 200 °C are 3.60, 0.47, and 1.15% for the nanorods, nanobelts, and nanoplates, respectively, which are attributed to the removal of adsorbed water. The mass loss of the nanorods at 200–800 °C of ca. 13.22% is due to the removal of structural water and the surface –OH groups from γ-AlOOH, which corresponds to the phase transformation from γ-AlOOH to γ-Al_2O_3,[25] whereas the mass losses of the nanobelts and nanoplates are 15.16 and 15.14%, respectively, which are higher than that of the nanorods and match well with the theoretical value of 15% on going from γ-AlOOH to γ-Al_2O_3. The

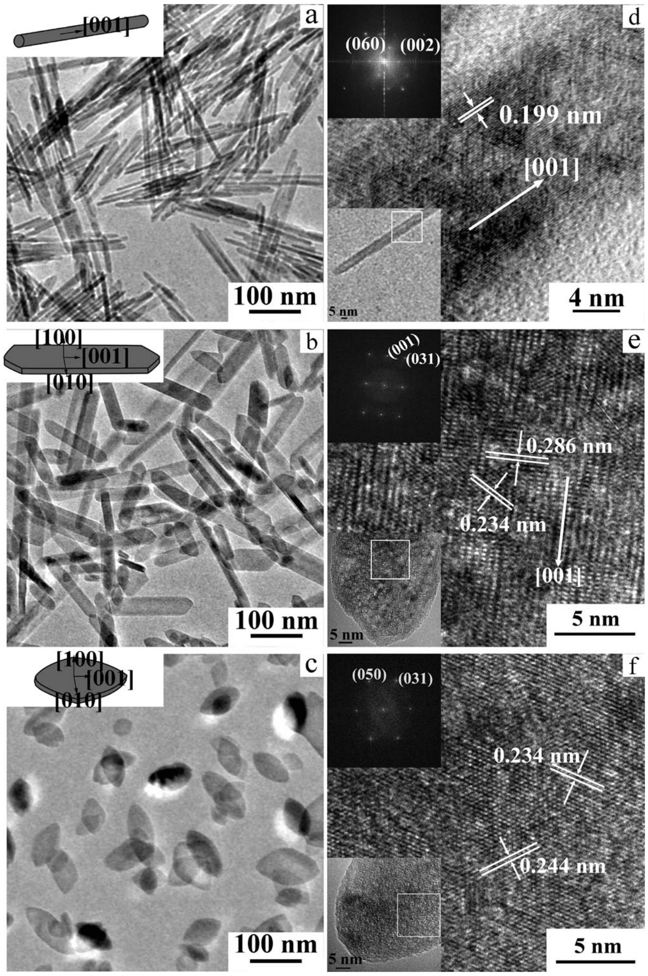

Figure 2. TEM and HRTEM images of the products formed in the presence of H_2SO_4 (a, d), CH_3COOH (b, e), and HCl (c, f). Inset in a, b, and c are the corresponding structure sketch maps, and those in d, e, and f are the corresponding FFT patterns.

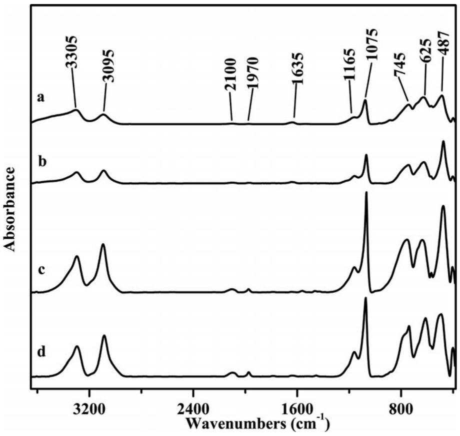

Figure 3. FTIR spectra of the raw material (a), nanorods (b), nanobelts (c), and nanoplates (d).

TGA curves of the nanobelts and nanoplates show small mass losses (0.95 and 1.18%, respectively) after 800 °C, which might be due to the removal of the surface –OH groups from γ-Al_2O_3. The TGA curve of the nanorods shows a 3.01% mass loss after 800 °C, which might be due to their larger surface area, which is in accordance with the larger mass loss of absorbed water before 200 °C.

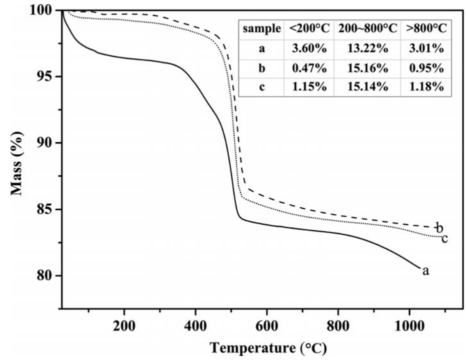

Figure 4. TGA curves of the nanorods (a), nanobelts (b), and nanoplates (c).

Large-scale experiments produce similar results, and the corresponding XRD patterns and TEM images are shown in Figure S2. The reflections of all the products from the large-scale syntheses were also indexed to the orthorhombic boehmite phase of γ-AlOOH, and those of the product from the large-scale H_2SO_4 system are also much weaker than the others. The TEM images of the products from the large-scale experiments are almost the same as the typical products discussed above.

Formation Mechanism of the Products

Time-dependent experiments were conducted to investigate the formation process of the γ-AlOOH nanomaterials. As shown in Figure 5, after the hydrothermal reaction at 240 °C in the presence of H_2SO_4 for 1 h, the majority of product was rice-grain-shaped particles with a length of ca. 10 nm, and a few of nanorods with a length of ca. 30 nm were observed. When the reaction was carried out for 2 h, nanorods with a diameter of 10 nm and a length of 50–100 nm were formed. With increased reaction time, the length of the nanorods obviously increased, and the diameter increased very slowly. For the CH_3COOH system, 15–60 nm irregular nanoplates and nanobelts with a length of 100 nm were obtained after a hydrothermal reaction of 1 h. On increasing the reaction time to 2 h, almost all of the nanoplates turned into nanobelts. Nanobelts with a width of 20–40 nm and a length of 60–250 nm were produced when the reaction time was prolonged to 3 h. When the reaction was conducted for 17 h, nanobelts with a width of 30–70 nm and a length of 100–800 nm were obtained (Figure 2). For the HCl system, after hydrothermal reaction of 1 h, 20–50 nm elliptical nanoplates were formed. On prolonging the reaction time to 2 h, the nanoplates grew larger, and the length/width ratio slightly decreased. Finally, quasi-square nanoplates with a side length of 55–155 nm were obtained (Figure 2).

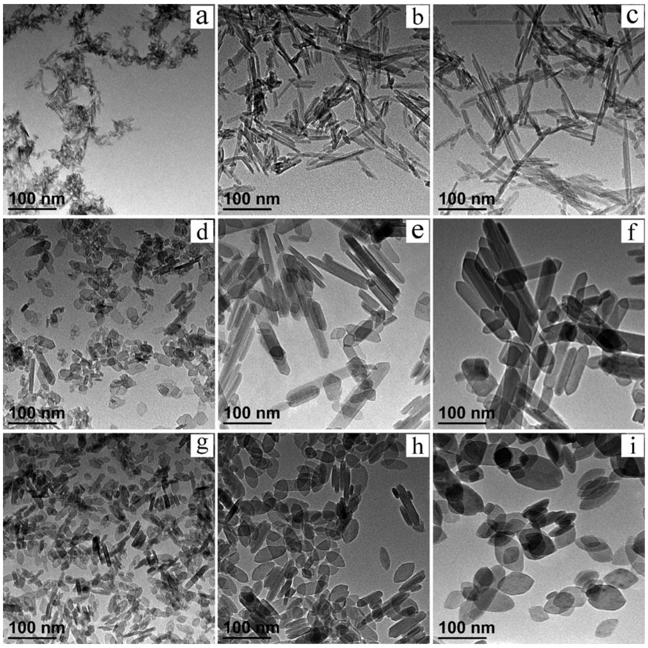

Figure 5. TEM images of the products from hydrothermal reaction systems at 240 °C for different times. H_2SO_4 system: 1 h (a), 2 h (b), 3 h (c); CH_3COOH system: 1 h (d), 2 h (e), 3 h (f); HCl system: 1 h (g), 2 h (h), 3 h (i).

Combining the time-dependent experiments with the HRTEM results, the γ-AlOOH nanoparticles aggregated and grew into different shapes under hydrothermal conditions in different acid systems. The –OH groups in the (0 1 0) and (1 0 0) facets could act as the adsorption site for acid anions through H-bonds;[8b] thus, the anions might selectively adsorb on the (0 1 0) and (1 0 0) facets.[8a] The adsorptions would decrease the surface energy and limit the aggregation of the γ-AlOOH nanoparticles on these facets, which would result in the aggregation of γ-AlOOH nanoparticles preferentially along the [0 0 1] direction. Obviously, the adsorption ability of the acid anions is related to the charge/size ratio, which affects the oriented aggregation, and the anions with the larger charge/size ratio would be adsorbed more easily on the particle surface of γ-AlOOH.[8a] The charge/size ratios for Cl^-, CH_3COO^-, and SO_4^{2-} are 4.348, 6.289, and 8.696, respectively, i.e. the order of the charge/size is $Cl^- < CH_3COO^- < SO_4^{2-}$,[26,27] and therefore, the order of the adsorption ability is $Cl^- < CH_3COO^- < SO_4^{2-}$. In analogy, the aspect ratio of the γ-AlOOH aggregates increased in the order of $Cl^- < CH_3COO^- < SO_4^{2-}$ with the aggregation rate of $Cl^- > CH_3COO^- > SO_4^{2-}$. Thus, the length of the aggregates along the [0 0 1] direction gradually decreased with the adsorption ability decreasing from SO_4^{2-} to CH_3COO^- and Cl^-.

In addition to aggregation, crystal growth based on Ostwald ripening occurred, which was mainly along the [0 0 1] and [0 1 0] directions. The driving force for the Ostwald ripening process is the reduction of total energy.[29] The Ostwald ripening process has become widely used in the preparation of nanoparticles, which is briefly described as the growth of larger crystals at the expense of smaller ones; i.e. smaller, less crystalline, or less dense particles in a colloidal aggregate will be dissolved gradually while larger, better crystallized, or denser particles grow in the same aggregate.[30,31] In our experiment, the same phenomenon appeared. In the time-dependent experiments with prolonged hydrothermal reaction times, especially from 1 to 2 h, the smaller particles gradually disappeared, and the larger particles became even larger (Figure 5).

With prolonged hydrothermal reaction times, desorption of the acid anions occurred, and the surface acid anions were gradually replaced by water molecules.[8a] The desorption order is the opposite to the adsorption order, i.e. $Cl^- > CH_3COO^- > SO_4^{2-}$. The influence of the acid anion is decreased in the Ostwald ripening process. In this case, the difference in the crystal plane energies is the key factor that influences the shape of the product. Mercuri et al. applied molecular dynamics simulations to investigate the boehmite/water surface energy and concluded that the surface energies of γ-AlOOH nanorods with growth directions of [0 0 1], [0 1 0], and [1 0 0] were 0.54, 0.59, and 0.90 J/mol,[28] respectively; i.e. the surface energy of γ-AlOOH was in the order of (0 0 1) > (0 1 0) > (1 0 0). This conclusion implied that γ-AlOOH would grow preferentially in the direction order [0 0 1] > [0 1 0] > [1 0 0] in aqueous solution. In our experiment, the acid anions desorbed in the order of $Cl^- > CH_3COO^- > SO_4^{2-}$. Cl^- desorbed rapidly, so the corresponding aggregates grew preferentially in the direction order of [0 0 1] > [0 1 0] > [1 0 0], and nanoplates with the (1 0 0) plane as the exposed surface formed from the HCl system. Desorption of CH_3COO^- was relatively slow, which partly limited the growth along the [0 1 0] and [1 0 0] directions, and nanobelts with dimensions in the order of [0 0 1] > [0 1 0] > [1 0 0] were formed. Due to the strong adsorption of SO_4^{2-} on the particle surfaces of γ-AlOOH, their desorptions could be omitted during the hydrothermal process, so growth along both the [1 0 0] and [0 1 0] directions was limited, and nanorods that grew along the [0 0 1] direction were obtained.

Figure 6 shows that the length of nanorods increased with increasing H_2SO_4 content, and the nanobelts became longer as the CH_3COOH content increased. When the HCl content was 20.0 mmol, the products exhibited irregular shapes, and as the HCl content reached 50.0 mmol, the diagonal length of the nanoplates lengthened. This demonstrates that increasing the acid content favored growth along the [0 0 1] direction.

As a comparison, the experiment was carried out in the absence of acid. SEM images (Figure S3) reveal that the product comprised irregular blocks with a wide size distribution. After hydrothermal reaction for 1 h, a mixture of nanoplates and nanoparticles was obtained, of which the majority was nanoplates. As the reaction time was prolonged to 2 h, irregular blocks were formed. Further experiments showed that it was difficult to obtain nanomaterials with regular shapes without acid; thus, the acid was the key factor that affected the shape of the product (Figure S4).

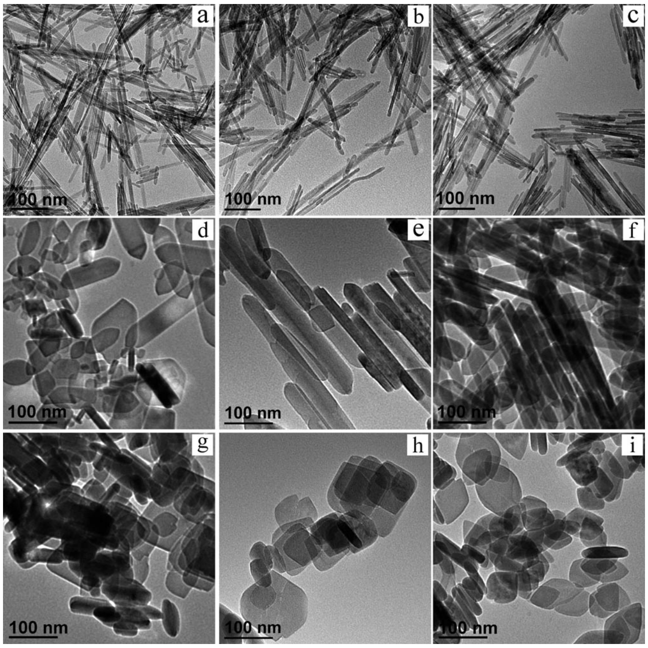

Figure 6. TEM images of the products formed by different contents of acids. H_2SO_4 system: 10.0 mmol (a), 21.5 mmol (b), 25.0 mmol (c); CH_3COOH system: 20.0 mmol (d), 43.0 mmol (e), 50.0 mmol (f); HCl system: 20.0 mmol (g), 43.0 mmol (h), 50.0 mmol (i).

Based on this analysis, the formation of nanorods, nanobelts, and nanoplates is based on oriented aggregation and Ostwald ripening. The acid anions adsorbed on the particular crystal planes direct the aggregation of the raw γ-AlOOH nanoparticles and the growth of their aggregates. The difference in the shapes of the products is attributed to the difference in the adsorption abilities of the acid anions. The proposed formation mechanism is shown in Figure 7.

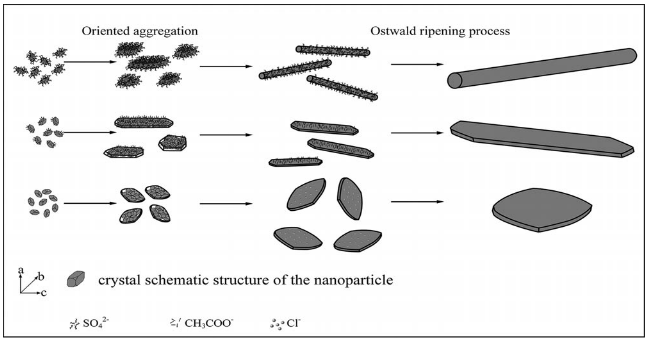

Figure 7. Schematic depiction of the proposed formation mechanism for the products.

The nanorods, nanobelts, and nanoplates were heated to 500 °C at a rate of 3 °C/min in air and kept at 500 °C for 3 h. The XRD patterns show that all the γ-AlOOH nanomaterials completely transform to γ-Al_2O_3 after calcination (JCPDS No.10-0425, Figure S5). The TEM images of the as-obtained γ-Al_2O_3 (Figure S6) demonstrate that the shapes of the γ-AlOOH nanomaterials are retained after calcination.

Adsorption Properties

The products derived from the same precursor and similar systems exhibit different morphologies and exposed facets, which provides the opportunity to investigate the effect of the exposed facet on the properties of the materials. Adsorption always occurs on the surface of the particles or the pores of the material; therefore, the adsorption of $Cr_2O_7^{2-}$ in aqueous solution of the obtained products was studied. Both the raw γ-AlOOH nanoparticles and the products could adsorb $Cr_2O_7^{2-}$ in aqueous solution. The absorbance spectra of the $Cr_2O_7^{2-}$ solutions after treatment with different γ-AlOOH nanomaterials are shown in Figure S7, and the corresponding percentage adsorptions are listed in Table 1. The nanomaterials show obvious shape-dependent adsorption capabilities for $Cr_2O_7^{2-}$, in which the nanobelts exhibit a percentage adsorption of 95.5%. In comparison with previous reports, the nanobelts show a superior adsorption capability for $Cr_2O_7^{2-}$.[2] It is well known that a large surface area is favorable for adsorption, but here the adsorption capabilities of the nanomaterials are not consistent with the surface area. As shown in Figure S8, the N_2 adsorption/desorption isotherms of the raw material and the products show hysteresis loops that indicate the presence of mesopores. The corresponding Barret–Joyner–Halenda (BJH) pore size distribution (PSD) curves (inset in Figure S8) indicate that only the raw material has a relatively narrow PSD, and the pore size of the products became larger with the growth of the particles, which were formed by the accumulation of particles. Brunauer–Emmett–Teller (BET) analyses indicate that the surface areas for the raw material, nanorods, nanobelts, and nanoplates are 322.3, 124.1, 16.9, and 12.1 m^2/g, respectively (Table 1). The surface area of the raw material is much larger than that of the products, whereas its percentage adsorption is only 76.6%, which is much lower than that of the nanobelts (95.5%) (Table 1). Of the products, the nanorods have the largest surface area but exhibit the lowest adsorption capability. The main difference in these nanomaterials is the different exposed crystal facets. Here, the raw material shows a variety of exposed facets in nearly the same ratio, only a small amount of (0 0 1) facets are exposed for the nanorods, and for the nanobelts and nanoplates the main exposed facets are (1 0 0). Further calculations gave the percentage adsorptions of the unit surface area. It can be seen that the nanobelts and nanoplates show nearly the same values, which are much larger than those of the nanoparticles and nanorods. This result indicates that the exposed facets greatly affect the adsorption capabilities of the materials, and the (1 0 0) facet of γ-AlOOH exhibits a high adsorption ability to $Cr_2O_7^{2-}$. This is consistent with the adsorption order of the different crystal facets for the acid anions.[8] When the exposed crystal facet is the same, the product with larger surface area would have the highest adsorption.

Table 1. Percentage adsorption and surface areas of the raw materials and products.

	Raw material	Nanorods	Nanobelts	Nanoplates
Percentage adsorption [%]	76.6	32.0	95.5	68.2
BET surface area [m^2/g]	322.3	124.1	16.9	12.1
Percentage adsorption of unit surface area [%/m^2]	1.19	1.29	28.25	28.20

Conclusions

The γ-AlOOH nanorods, nanobelts, and nanoplates were prepared by a hydrothermal process in the presence of H_2SO_4, CH_3COOH, and HCl without organic additives or surfactants on a large scale. The formation of the products went through the oriented-aggregation and Ostwald ripening growth processes. The acid anions adsorbed on the particular crystal planes affected the aggregation of the raw γ-AlOOH nanoparticles and the growth of their aggregates. The shape differences of the products were attributed to the different adsorption abilities of the acid anions. After the γ-AlOOH nanorods, nanobelts, and nanoplates were calcined in air, the corresponding γ-Al_2O_3 nanomaterials with the same shapes were obtained. The nanomaterials have different adsorption capabilities for $Cr_2O_7^{2-}$ in aqueous solution, and the nanobelts exhibit the highest percentage adsorption of 95.5%. The exposed crystal facet of the γ-AlOOH nanomaterials is an important factor on the adsorption ability. The high yields obtained and the good adsorption properties of the nanobelts make it potentially applicable to waste water treatment.

Experimental Section

Materials: γ-AlOOH nanoparticles with a size of 2–5 nm (Shandong Aluminum Corporation) were used as the raw material, and their corresponding XRD pattern and TEM image are shown in Figure S1. All other chemical reagents were of analytical grade and used without further purification.

Preparation: In a typical synthesis, γ-AlOOH nanoparticles (33.5 g, 0.6 mol) were added to water (366.5 mL), the mixture was stirred vigorously for 60 min to form a well-dispersed suspension, and an aqueous solution (5.0 mL) containing H_2SO_4 (21.5 mmol), CH_3COOH (43.0 mmol) or HCl (43.0 mmol) was added. The suspension was poured into a Teflon-lined stainless-steel autoclave and heated at 240 °C for 17 h. After the autoclave had cooled naturally to room temperature, the white product was separated by centrifugation and washed with deionized water and ethanol. Finally, the product was dried at 100 °C for 24 h. The experiment could be scaled up to prepare γ-AlOOH (3.0 kg, 50.0 mol) products in one reaction.

Adsorption Experiments: Adsorption experiments were carried out in batch mode by mixing a γ-AlOOH sample (0.2 g) with an aqueous solution (20.0 mL) of $K_2Cr_2O_7$ (1×10^{-4} mol L^{-1}) in a stoppered Erlenmeyer flask (50.0 mL). The Erlenmeyer flask was shaken with a rotary shaker at 130 rpm for 4 h. After shaking, the suspension was immediately centrifuged to remove the γ-AlOOH, the $Cr_2O_7^{2-}$ concentration in the filtrate was determined with a UV/Vis spectrometer (Lambda-35, Perkin–Elmer) at λ = 550 nm by using the diphenylcarbazide method. The percentage of $Cr_2O_7^{2-}$ adsorbed by γ-AlOOH was determined as the difference between the initial $[C]_\mathrm{i}$ and final $[C]_\mathrm{f}$ $Cr_2O_7^{2-}$ concentration in the solution. Equation (1) was used to calculate the adsorption percentage of $Cr_2O_7^{2-}$.[2]

$$\%\ \text{adsorption} = \frac{[C]_\mathrm{i} - [C]_\mathrm{f}}{[C]_\mathrm{i}} \times 100 \qquad (1)$$

All the experiments were carried out at room temperature (25 °C), and the pH value of the solution was 5.5.

Instrumentation: The crystal structure of the products was determined by X-ray diffraction (XRD) patterns collected with a Rigaku D/Max 2200PC diffractometer using a graphite monochromator (Cu-K_α radiation, λ = 0.15418 nm, tube voltage and electric current: 40 kV and 20 mA). The shape and microstructure were characterized with a field emission SEM (FE-SEM, JEOL JSM-6700F and TOSHIBA S4800), TEM (TEM, JEM-100CXII) with an accelerating voltage of 80 kV, and HRTEM (HR-TEM, JEOL JEM-2100, and JEM-2010) with an accelerating voltage of 200 kV. FTIR spectra were measured with a Nicolet 5DX-FTIR spectrometer in the range of 400–4000 cm^{-1} by using a KBr pellet. TGA was employed to evaluate the mass loss of the sample under an air flow of 20.0 mL/min and a heating rate of 10.0 °C/min by using a thermal analyzer (Mettler Toledo SDTA851$^\mathrm{e}$). The BET surface area (S_BET) was measured with the N_2 adsorption technique at 77 K with a QuadraSorb SI surface area analyzer after degassing the samples at 180 °C for 8.0 h.

Supporting Information (see footnote on the first page of this article): XRD patterns and TEM images of the raw material, large-scale experiment products, products in the absence of acid and products after calcination, absorbance spectra of $Cr_2O_7^{2-}$ solutions after treatment with the raw material and products, N_2 adsorption/desorption isotherms, and BJH pore size distribution curves of the raw material and products.

Acknowledgments

This work was supported by the Major State Basic Research Development Program of China (973 Program) (No. 2010CB933504), the Science Funds for Distinguished Young Scientists of Shandong Province (JQ200903), and the Natural Science Foundation of Shandong Province (No. ZR2011BZ002).

---

[1] A. Dandapat, G. De, *J. Mater. Chem.* **2010**, *20*, 3890–3894.

[2] F. Granados-Correa, J. Jiménez-Becerril, *J. Hazard. Mater.* **2009**, *162*, 1178–1184.

[3] a) W. Brostow, T. Datashvili, D. Kao, J. Too, *Polym. Compos.* **2010**, *31*, 417–425; b) J. Górka, P. F. Fulvio, S. Pikus, M. Jaroniec, *Chem. Commun.* **2010**, *46*, 6798–6800.

[4] S. C. Shen, Q. Chen, P. S. Chow, G. H. Tan, X. T. Zeng, Z. Wang, R. B. H. Tan, *J. Phys. Chem. C* **2007**, *111*, 700–707.

[5] X. Y. Chen, H. S. Huh, S. W. Lee, *Nanotechnology* **2007**, *18*, 285608–285612.

[6] L. M. Zhang, W. C. Lu, L. M. Yan, Y. L. Feng, X. H. Bao, J. P. Ni, X. F. Shang, Y. Lv, *Microporous Mesoporous Mater.* **2009**, *119*, 208–216.

[7] a) Y. Y. Zhao, W. N. Martens, T. E. Bostrom, H. Y. Zhu, R. L. Frost, *Langmuir* **2007**, *23*, 2110–2116; b) Y. Y. Zhao, R. L. Frost, W. N. Martens, H. Y. Zhu, *Langmuir* **2007**, *23*, 9850–9859; c) H. Y. Zhu, X. P. Gao, D. Y. Song, Y. Q. Bai, S. P. Ringer, Z. Gao, Y. X. Xi, W. Martens, J. D. Riches, R. L. Frost, *J. Phys. Chem. B* **2004**, *108*, 4245–4247; d) Y. Y. Zhao, R. L. Frost, *J. Colloid Interface Sci.* **2008**, *326*, 289–299.

[8] a) T. B. He, L. Xiang, S. L. Zhu, *CrystEngComm* **2009**, *11*, 1338–1342; b) T. B. He, L. Xiang, S. L. Zhu, *Langmuir* **2008**, *24*, 8284–8289.

[9] Y. Y. Zhao, R. L. Frost, W. N. Martens, *J. Phys. Chem. C* **2007**, *111*, 5313–5324.

[10] X. Y. Chen, Z. J. Zhang, X. L. Li, S. W. Lee, *Solid State Commun.* **2008**, *145*, 368–373.

[11] a) T. Z. Ren, Z. Y. Yuan, B. L. Su, *Langmuir* **2004**, *20*, 1531–1534; b) L. Zhang, Y. J. Zhu, *J. Phys. Chem. C* **2008**, *112*, 16764–16768; c) X. X. Yu, J. G. Yu, B. Cheng, M. Jaroniec, *J. Phys. Chem. C* **2009**, *113*, 17527–17535; d) T. Kim, H. B. Li, J. B. Lian, H. H. Jin, J. M. Ma, X. C. Duan, G. Yao, W. J. Zheng, *Cryst. Res. Technol.* **2010**, *45*, 767–770; e) Y. L. Feng, W. C. Lu, L. M. Zhang, X. H. Bao, B. H. Yue, Y. Lv, X. F. Shang, *Cryst. Growth Des.* **2008**, *8*, 1426–1429; f) W. Q. Cai, J. G. Yu, S. H. Gu, M. Jaroniec, *Cryst. Growth Des.* **2010**, *10*, 3977–3982.

[12] a) B. Tang, J. C. Ge, L. H. Zhuo, G. L. Wang, J. Y. Niu, Z. Q. Shi, Y. B. Dong, *Eur. J. Inorg. Chem.* **2005**, 4366–4369; b) H. Liang, L. Liu, Z. J. Yang, Y. Z. Yang, *Cryst. Res. Technol.* **2010**, *45*, 195–198; c) Y. Zhu, H. W. Hou, G. L. Tang, Q. Y. Hu, *Eur. J. Inorg. Chem.* **2010**, 872–878; d) W. Q. Cai, J. G. Yu, M. Jaroniec, *J. Mater. Chem.* **2010**, *20*, 4587–4594; e) X. Yang, J. Y. Wang, H. Y. Pan, *J. Nanosci. Nanotechnol.* **2009**, *9*, 1123–1126; f) Y. Y. Zhao, R. L. Frost, *J. Nanosci. Nanotechnol.* **2009**, *9*, 3181–3187; g) W. Q. Cai, J. G. Yu, B. Cheng, B. L. Su, M. Jaroniec, *J. Phys. Chem. C* **2009**, *113*, 14739–14746; h) Y. Mathieu, B. Lebeau, V. Valtchev, *Langmuir* **2007**, *23*, 9435–9442.

[13] a) F. Rashidi, A. N. Kharat, A. M. Rashidi, E. Lima, V. Lara, J. S. Valente, *Eur. J. Inorg. Chem.* **2010**, 1544–1551; b) X. Bokhimi, A. Morales, J. S. Valente, *J. Phys. Chem. C* **2007**, *111*, 103–107; c) M. M. Amini, M. Mirzaee, *J. Sol-Gel Sci. Technol.* **2005**, *36*, 19–23; d) M. Nguefack, A. F. Popa, S. Rossignol, C. Kappenstein, *Phys. Chem. Chem. Phys.* **2003**, *5*, 4279–4289; e) S. C. Kuiry, E. Megen, S. D. Patil, D. S. A. Eshpande, S. Seal, *J. Phys. Chem. B* **2005**, *109*, 3868–3872.

[14] T. Kim, J. B. Lian, J. M. Ma, X. C. Duan, W. J. Zheng, *Cryst. Growth Des.* **2010**, *10*, 2928–2933.

[15] D. B. Kuang, Y. P. Fang, H. Q. Liu, C. Frommen, D. Fenske, *J. Mater. Chem.* **2003**, *13*, 660–662.

[16] M. Antonietti, G. A. Ozin, *Chem. Eur. J.* **2004**, *10*, 28–41.

[17] R. Bardhan, O. Neumann, N. Mirin, H. Wang, N. J. Halas, *ACS Nano* **2009**, *3*, 266–272.

[18] a) J. F. Banfield, S. A. Welch, H. Z. Zhang, T. T. Ebert, R. L. Penn, *Science* **2000**, *289*, 751–754; b) R. L. Penn, J. F. Banfield, *Science* **1998**, *281*, 969–971; c) R. L. Penn, J. F. Banfield, *Geochim. Cosmochim. Acta* **1999**, *63*, 1549–1557.

[19] Q. Zhang, S. J. Liu, S. H. Yu, *J. Mater. Chem.* **2009**, *19*, 191–207.

[20] C. Pacholski, A. Kornowski, H. Weller, *Angew. Chem.* **2002**, *114*, 1234; *Angew. Chem. Int. Ed.* **2002**, *41*, 1188–1191.

[21] W. L. Suchanek, J. M. Garcés, *CrystEngComm* **2010**, *12*, 2996–3002.

[22] D. Wang, J. Li, X. Cao, G. S. Pang, S. H. Feng, *Chem. Commun.* **2010**, *46*, 7718–7720.

[23] J. Y. Feng, M. C. Yin, Z. Q. Wang, S. C. Yan, L. J. Wan, Z. S. Li, Z. G. Zou, *CrystEngComm* **2010**, *12*, 3425–3429.

[24] G. Krishna Priya, P. Padmaja, K. Warrier, A. Damodaran, G. Aruldhas, *J. Mater. Sci. Lett.* **1997**, *16*, 1584–1587.

[25] A. M. de Aguilar Cruz, J. G. Eon, *Appl. Catal. A* **1998**, *167*, 203–213.

[26] L. P. Méndez De Leo, R. H. Wood, *J. Phys. Chem. B* **2005**, *109*, 14243–14250.

[27] *Inorganic Chemistry* (Eds.: X. Z. Cao, T. Y. Song, X. Q. Wang), Higher Education Press, Peking, **1992**, chapter 4, p. 130.

[28] F. Mercuri, D. Costa, P. Marcus, *J. Phys. Chem. C* **2009**, *113*, 5228–5237.

[29] P. W. Voorhees, *J. Stat. Phys.* **1985**, *38*, 231–252.

[30] B. P. Jia, L. Gao, *Cryst. Growth Des.* **2008**, *8*, 1372–1376.

[31] J. Li, H. C. Zeng, *J. Am. Chem. Soc.* **2007**, *129*, 15839–15847.

Received: July 29, 2011